J Solid State Electrochem (2009) 13:869–878
DOI 10.1007/s10008-008-0616-1

ORIGINAL PAPER

Comparative study of different indigo-clay Maya Blue-like systems using the voltammetry of microparticles approach

Antonio Doménech · María Teresa Doménech-Carbó · Manuel Sánchez del Río · María Luisa Vázquez de Agredos Pascual

Received: 12 May 2008 / Revised: 12 June 2008 / Accepted: 12 June 2008 / Published online: 15 July 2008

Abstract Using the voltammetry of microparticles approach, the electrochemical response of complexes prepared with indigo plus different clays in contact with aqueous electrolytes is described. Indigo presents a strong attachment with palygorskite and sepiolite in contrast to a weak attachment to planar clays (montomorillonite and kaolinite). Cyclic voltammetric and chronoamperometric data provide estimates of the variation of the concentration of indigo and dehydroindigo with the depth on clay crystals. The indigoids (indigo and dehydroindigo) penetrate more in palygorskite than in sepiolite, and this penetration is favoured by thermal treatments (very efficient up to 130 °C). The indigo concentration decreases monotonically versus depth, while the dehydroindigo one increases from zero in the external region of the crystals to a maximum at a depth between 40 and 80 nm and then decreasing rapidly. These facts are directly linked to the much higher resistance to acid attack of palygorskite–indigo pigments (Maya Blue) than sepiolite–indigo ones.

A. Doménech (✉)
Departament de Química Analítica, Universitat de València,
Dr. Moliner, 50,
46100 Burjassot, València, Spain
e-mail: antonio.domenech@uv.es

M. T. Doménech-Carbó · M. L. V. de Agredos Pascual
Institut de Conservació del Patrimoni/Departament de Conservació i Restauració de Bens Culturals,
Universitat Politécnica de València,
Camí de Vera 14,
46022 València, Spain

M. S. del Río
European Synchroton Radiation Facility,
BP220, 38043 Grenoble Cedex, France

Keywords Maya Blue · Indigo · Palygorskite · Sepiolite · Montmorillonite · Kaolinite · Solid-state electrochemistry · Organic–inorganic hybrid pigment

Introduction

Maya Blue is a famous artificial pigment widely used in murals, pottery and sculptures by the ancient Mayas and other people in Mesoamerica [1]. The pigment, whose hue ranges from bright turquoise to dark greenish blue, exhibits a remarkable stability, being unaffected by the attack of acids, alkalis, oxidants, reducing agents, organic solvents, as well as biodegradation.

Maya Blue can be described as a hybrid organic–inorganic material [2] resulting from the association of indigo (H_2IN=3H-indol-3-one, 2-(1,3-dihydro-3-oxo-2H-indol-2-ylidene)-1,2-dihydro), a blue dye extracted from *Indigofera suffruticosa* and other plants, to a local clay, palygorskite (known as attapulgite for historians and restorers), a fibrous phyllosilicate [1].

The nature of the indigo–palygorskite association and the reasons for its hue and durability have become controversial [3–15]. Shepard [3] first introduced the idea of Maya Blue being an unusual pigment consisting on a dye attached to certain clays in Yucatan. In 1966, Van Olphen [4] prepared a complex analogous to Maya Blue by heating indigo with palygorskite or sepiolite, both clays with fibrous structure. Pigments prepared with indigo plus laminar silicates were found to be non-resistant to acidic attack. Val Olphen suggested that indigo molecules are too large to enter into the channels of the clay, so that such channels are in some way sealed at their ends by indigo molecules [4]. Kleber et al., however, proposed that partial

or even deep penetration of indigo molecules inside the palygorskite channels is possible [5].

A significant part of recent studies are focused on the nature of the indigo–palygorskite association. Recent hypothesis include anchoring of indigo molecules to the openings of the clay channels by means of hydrogen bonds of carbonyl and amino groups to silanol units bordering the clay micropores [11], hydrogen bonding between C=O and N–H groups of indigo molecules and structural water molecules inside palygorskite channels [10, 14, 15], hydrogen bond between indigo carbonyl and structural water with participation of a direct interaction between indigo and clay octahedral cations, not mediated by structural water, accompanied by Van der Waals interactions [12].

In previous works, Maya Blue samples from different Mexican archaeological sites in Yucatán and Campeche and synthetic indigo plus palygorskite specimens have been studied by means of voltammetry of microparticles combined with spectroscopic and microscopic techniques [16–19]. This methodology, developed by Scholz et al.[20–22], provides information of the redox reactivity of insulating, sparingly soluble solids, upon recording their voltammetric response in contact with suitable electrolytes. As a result, it was suggested that dehydroindigo, the oxidized form of indigo, accompanies indigo in the palygorskite–indigo complex thus modulating the hue of Maya Blue [16]. Thermochemical data concerning the association to such molecules to the clay support were also obtained [16, 18]. The analysis of the electrochemical data complemented with other spectroscopy data also suggested that the ancient recipe for the preparation of indigo [19] and Maya Blue [18] evolved with time.

With the aim of obtaining information on the nature of the chemical interaction between palygorskite and indigo in Maya Blue, it is described here a voltammetry of microparticles study performed on indigo combined with different clays. These clays are: palygorskite from the classical site of Sacalum [23], sepiolite, montmorillonite and kaolinite. Palygorskite, whose ideal formula is $Si_8O_{20}Al_2Mg_2(OH)_2(H_2O)_4{\cdot}4H_2O$, can be described as a mixture of two different polytypes: one monoclinic and one orthorombic [24], both consisting of ribbons of 2:1 phyllosilicated tetrahedral/octahedral linked by periodical inversion of the apical oxygen in the continuous sheet of SiO_4 tetrahedra. This gives rise to a series of rectangular tunnels of dimensions 6.4×3.7 Å. Sepiolite is a fibrous aluminosilicate of theoretical formula $Si_6Mg_4O_{15}(OH)_2{\cdot}6H_2O$ similar to palygorskite, presenting 10.6×3.7-Å-sized tunnels [25]. Such clays are therefore crossed by zeolite-like channels and permeated by weakly bound, non-structural (zeolitic) water. Aluminium and magnesium cations complete their coordination with tightly bound water molecules (structural water). Montmorillonite ($(Na,Ca)_{0.33}(Al,Mg)_2Si_4O_{10}(OH)_2{\cdot}nH_2O$) and kaolinite ($Al_2Si_2O_5(OH)_4$) are representative of planar clays. Previous works of Sánchez del Río et al. [22, 23] have shown that: (1) palygorskite-based pigments become much more resistant tan sepiolite-based ones with regard to acid attack [26] and (2) montmorillonite and kaolinite produce a weak interaction with indigo leading to some spectral features in Raman spectra similar to that of palygorskite–indigo and sepiolite–indigo ones [27].

Here, the electrochemistry of pigment specimens prepared by crushing synthetic indigo and the corresponding clay and submitted to different thermal treatments is described upon attachment to paraffin-impregnated graphite electrodes (PIGEs). Cyclic and square wave voltammetries (CV and SWV, respectively) and chronoamperometry (CA) have been used in order to gain information on: (1) variations with the clay nature in the indigo–clay attachment, (2) variation of the indigo concentration within the clay crystals, (3) determination of the presence of dehydroindigo and eventually the variation of the dehydroindigo/indigo ratio with the depth within clay crystals.

Experimental

Palygorskite was collected from Yucatán (Mexico) sites of Sacalum (P1) and Ticul (P2). Sepiolite from Yunclillos (Spain) was supplied by Tolsa, and it is presented in mineral form (S1) or in finely grinded commercial material (S2). Montmorillonite from Wyoming (MW) was obtained through the Source Clays Repository of the Clay Mineral Society, while kaolinite (K) was a commercial simple (North). A first series of Maya Blue-type specimens (respectively, MBP1, MBP2, MBS1, MBS2, MBMW, MBK) were prepared by finely grinding and mixing 1.5% (*w*/*w*) of synthetic indigo (Fluka) with the clay in an agate mortar and pestle during 30 min. Three additional series of specimens were prepared from aliquots of the above ones by submitting specimens to heating at 110, 150 and 180 °C during 24 h. These series will be labelled as $MBP1_t$, $MBP2_t$, $MBS1_t$, $MBS2_t$, MBM_t and MBK_t, with t=110, 150 and 180 °C, respectively. In order to eliminate interferences from non-clay-attached indigo, specimens were suspended in dimethyl sulphoxide (DMSO) and ultrasonicated for 15 min. After decantation, the resulting powders were repeatedly rinsed with acetone and dried in air.

Voltammetry of microparticles experiments were performed using PIGEs immersed into 0.50 M sodium acetate buffer, pH 4.75, prepared in nanopure water with acetic acid (99.8%, Fluka) and sodium acetate trihydrate (99.5%, Fluka). Measurements were performed in a thermostated three-electrode cell under argon atmosphere using a AgCl (3 M NaCl)/Ag reference electrode and a platinum-wire auxiliary electrode. CV, SWV and CA experiments were performed with a CH I420 (Cambria Scientific, UK) equipment.

For modified electrode preparation, the samples were thoroughly powdered in an agate mortar and pestle and extended forming a spot of finely distributed material. The lower end of the graphite electrode was pressed over that spot of sample to obtain a sample-modified surface.

Results and discussion

Voltammetric pattern

MBP1, MBP2, MBS1, MBS2, MBMW and MBK specimens consisted of granular materials with a blue hue. Sepiolite- and palygorskite-based specimens submitted to thermal treatments changed colour from blue to a greenish-blue on increasing temperature, while montmorillonite- and kaolinite-based materials remained essentially unchanged. After rinsing with DMSO and acetone, all montmorillonite- and kaolinite-based specimens become decoloured, thus denoting that a weak attachment of indigo to such clays occurs. In contrast, palygorskite- and sepiolite-based specimens maintained their blue or blue-greenish hue.

Figure 1 shows the SWV response of: (a) MBP1, (b) MBS1 and (c) MBMW, attached to PIGEs in contact with 0.50 M acetate buffer (pH 4.75). On scanning the potential from −0.65 V in the positive direction, well-defined peaks at +0.45 (I) and −0.28 V (II) vs. AgCl/Ag appear in all cases, superimposed to a series of overlaping peaks in the +0.30 to −0.20 V potential range. These last peaks were also found in SWVs of indigo-free clays, thus being attributable to quinone functionalities produced in the graphite surface. As described in literature [28–32], such quinone functionalities can be promoted by scratching of the graphite surface, thus yielding relatively intense voltammetric peaks.

The peak potential for processes I and II remained essentially frequency independent in all cases, suggesting that both electrochemical processes behave almost reversibly. In contrast, the variation of the peak currents with the square wave frequency, f, was significantly different for the different specimens. These differences can be seen in Fig. 2 where the quotient between the peak currents of peaks I and II, $i_p(I)/i_p(II)$, with f are shown. For MBP1 and MBP2, the $i_p(I)/i_p(II)$ ratio slowly increases with frequency, while for MBS1, MBS2, MBMW and MBK, this ratio decreases monotonically on increasing f (see Fig. 2a).

The voltammetry of Maya Blue-type specimens prepared with montmorillonite and kaolinite and submitted to thermal treatment was essentially identical to that of untreated specimens. Similarly, $MBP1_{110}$, $MBP2_{110}$ and $MBS1_{110}$ specimens exhibited voltammetric responses essentially identical to those of MBP1, MBP2, MBS1 and MBS2, respectively. Remarkably, sepiolite-based specimens treated

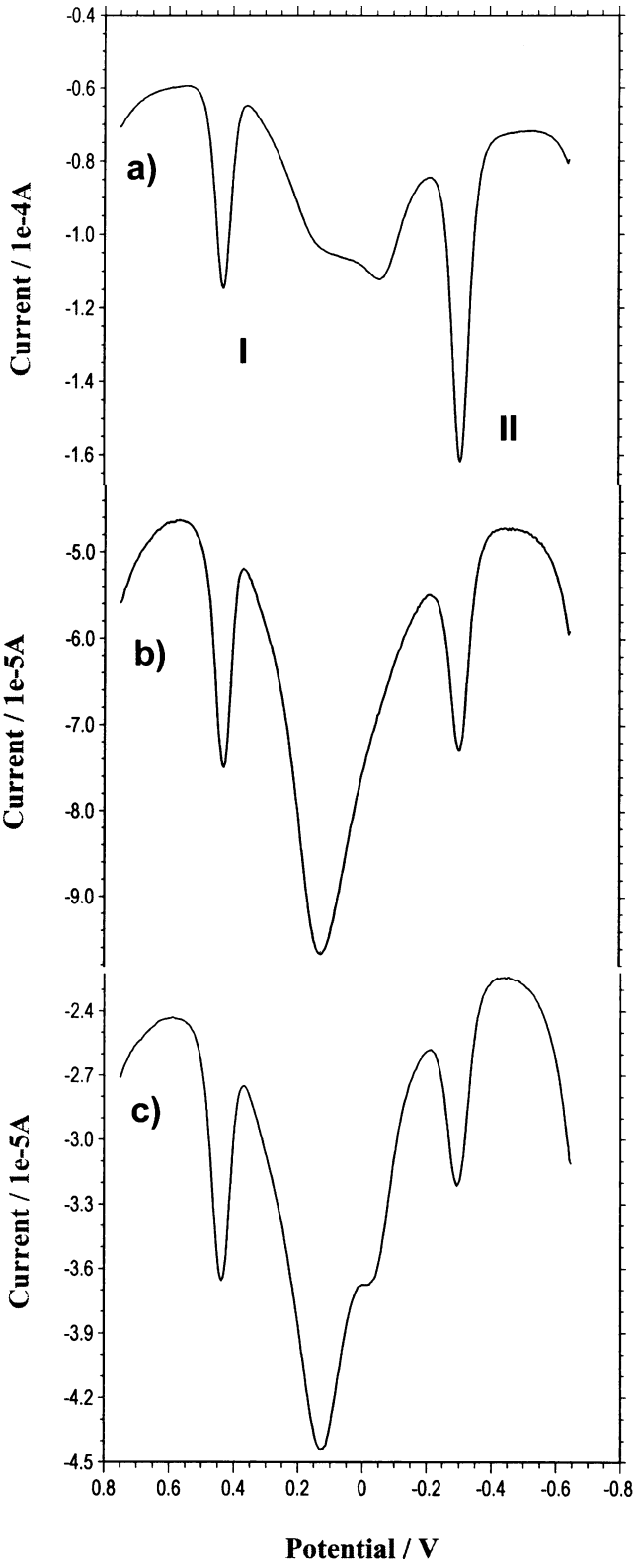

Fig. 1 SWVs for synthetic specimens: **a** MBP1, **b** MBS1 and **c** MBMW, attached to PIGEs in contact with 0.50 M acetate buffer (pH 4.75). Potential scan initiated at −0.65 V in the positive direction. Potential step increment 4 mV; square wave amplitude 25 mV; frequency 50 Hz

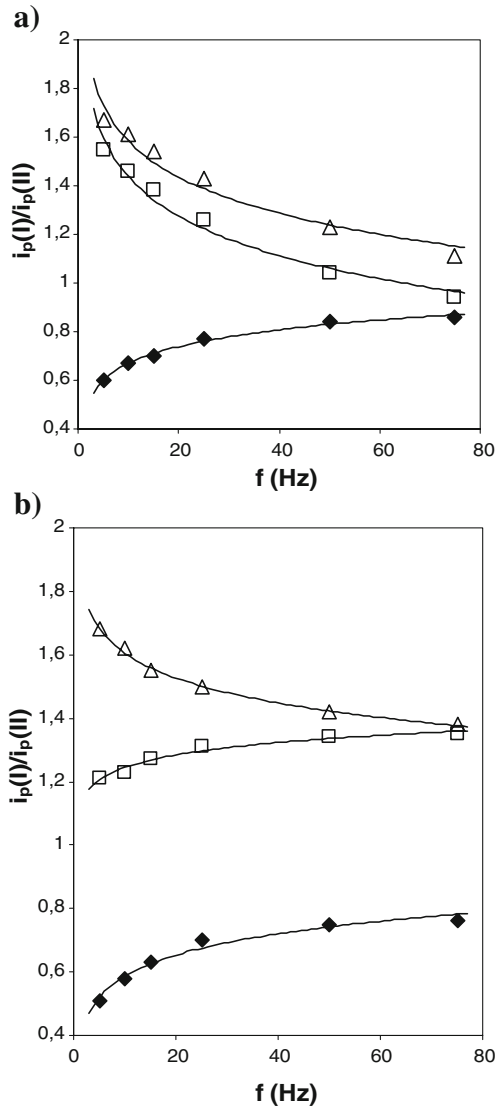

Fig. 2 Plots of $i_p(I)/i_p(II)$ vs. f for: **a** MBP1 (*rhombs*), MBS1 (*squares*) and MBMW (*triangles*); **b** $MBP2_{150}$ (*rhombs*), $MBS1_{150}$ (*squares*) and MBW_{150} (*triangles*), all in contact with 0.50 M acetate buffer (pH 4.75). Potential scan initiated at −0.65 V in the positive direction. Potential step increment 4 mV; square wave amplitude 25 mV

at 150 and 180 °C produced significant differences with respect to untreated ones. In the case of sepiolite specimens, the variation of peak currents with the square wave frequency changed, and it was found to be similar to that previously described for palygorskite-based specimens. This can be seen in Fig. 2b, where the variation of the $i_p(I)/i_p(II)$ ratio on the square wave frequency for $MBP1_{150}$, $MBS1_{150}$ and $MBMW_{150}$ is shown.

After rinsing with DMSO and acetone, all kaolinite- and montmorillonite-based specimens become discoloured, and no significant indigo-localized signals were recorded in voltammetric experiments. In contrast, palygorskite- and sepiolite-based specimens maintained blue-greenish hue after rinsing with DMSO and acetone. Then, voltammetric measurements were similar to those previously described. Remarkably, in the case of $MBP1_{150}$ and $MBP1_{180}$ specimens, the peak I is resolved into two peaks at +0.37 and +0.43 V and accompanied by an additional peak at +0.62 V (III). As can be seen in Fig. 3, where SWVs for $MBP1_{150}$ at (a) 5 and (b) 50 Hz are shown, peak splitting disappears on increasing square wave frequency. Remarkably, peak splitting was not observed for sepiolite-based specimens.

These features can be rationalized on the basis of literature dealing with the voltammetry of indigo microparticles [19, 33–35] and Maya Blue samples [16–18] attached to graphite electrodes, assuming that different types of attachment of indigo to the clay may exist. This situation parallels to that described for zeolite-associated species, for which different so-called topological redox isomers display discernable electrochemical responses [36–38]. Accordingly, voltammetric peaks I and II can unambiguously be attributed, respectively, to the oxidation of indigo, H_2IN, to dehydroindigo, IN (peak I), and the reduction of indigo to leucoindigo, H_4IN (peak II). In the case of montmorillonite- and kaolinite-based specimens, such electrochemical processes can be represented as:

$$(H_2IN)_{ads} \rightarrow (IN)_{ads} + 2H^+(aq) + 2e^- \quad (1)$$

$$(H_2IN)_{ads} + 2H^+(aq) + 2e^- \rightarrow (H_4IN)_{ads} \quad (2)$$

In these equations, $(\ )_{ads}$ denotes species adsorbed onto the corresponding clay.

In the case of sepiolite- and palygorskite-based specimens, the above response is superimposed to that of indigo molecules firmly anchored to the clay. Then, voltammetric peaks I and II can be represented, respectively, as:

$$\{H_2IN\} \rightarrow \{IN\} + 2H^+(aq) + 2e^- \quad (3)$$

$$\{H_2IN\} + 2H^+(aq) + 2e^- \rightarrow \{H_4IN\} \quad (4)$$

where { } denotes species attached to the inorganic support. Notice that charge conservation is ensured in both cases by the issue/ingress of two protons and two electrons from/to the solid matrix to/from the electrolyte.

The differences observed between palygorskite- and sepiolite-based specimens and the corresponding specimens heated at 150 and 180 °C clearly suggest that thermal treatment results in a more strong attachment especially in the case of sepiolite.

The variation of the voltammetric pattern with the square wave frequency for heated palygorskite-based specimens depicted in Fig. 3 can be interpreted using the scheme previously developed for different electroactive species associated to zeolites and mesoporous aluminosilicates

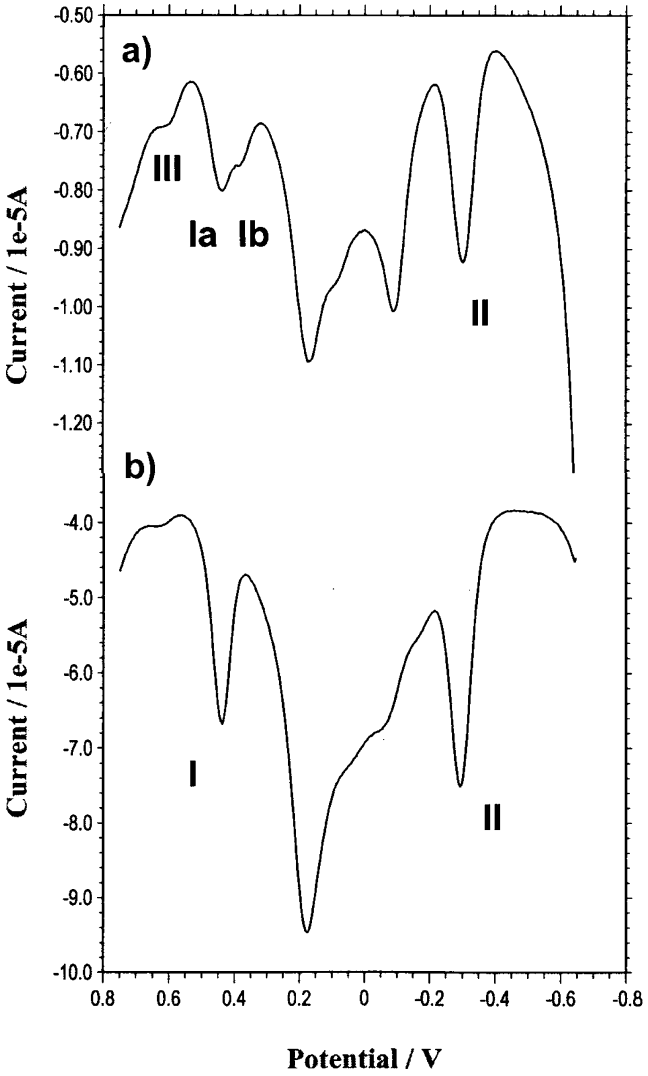

Fig. 3 SWVs for $MBP1_{150}$-modified PIGE in contact with 0.50 M acetate buffer (pH 4.75). Potential scan initiated at −0.65 V in the positive direction. Potential step increment 4 mV; square wave amplitude 25 mV; frequency: **a** 5, **b** 50 Hz

[37, 38]. At relatively long-time experiments (roughly, low frequencies), the electrochemical response reflects the behaviour of molecules strongly attached to the inorganic matrix, while at relatively short-time experiments (high frequencies), the response of externally adsorbed and weakly associated molecules prevails. Then, peak splitting for process I at low square wave frequencies (see Fig. 3) can be taken as representative of the presence of two different topological indigo isomers strongly associated to the palygorskite framework.

Chronoamperometry

Chronoamperometric experiments were performed in order to correlate electrochemical data for Maya Blue-type specimens and theory for the voltammetry of immobilized microcrystals developed by Lovric, Scholz, Oldham and co-workers [39–42]. In this model, the redox process initiates at the solid particle/electrode/electrolyte three-phase junction and extends to the solid particle via electron hopping between adjacent, immobile redox centres and ion transport through the solid. In the case of microporous aluminosilicates, ion transport is facilitated by the occurrence of pores and channels [43]. As described by Schröder et al. [42], the chronoamperometric current for a deposit of N cuboid microparticles at short times satisfies a current (i)–time (t) relationship given by:

$$i = nFNc\left[pg\left(\frac{D_e^{1/2}+D_H^{1/2}}{2t^{1/2}}\right)+p(D_eD_H)^{1/2}-4D_H(2D_et)^{1/2}\right] \quad (5)$$

where D_e, D_H represent the coefficients of diffusion of electrons and protons in the solid (cm^2/s), n is the number of electrons involved in the redox reaction, c represents the concentration (mol/cm^3) of the electroactive centres in the solid, p represents the perimeter of the electrode/microcrystal junction of the cuboid, N the number of cuboids and g a length depending on the shape and size distribution of particles, related with the size of the three-phase junction boxes in which the crystal is divided for applying simulation procedures.

According to Eq. 5, the chronoamperometric current (i) can be described in terms of the sum of three contributions: a 'ordinary,' Cottrell-type $i \propto t^{-1/2}$ term, a time-independent term, associated to the finite size of the crystals, and a third term characterized by $i \propto t^{1/2}$, attributable to a edge effect also associated to the crystals [42]. For our purposes, it is convenient to use the function $it^{1/2}$, thus rewriting Eq. 1 in an abbreviated form as:

$$it^{1/2} = A = Bt^{1/2} - Ct \quad (6)$$

where the coefficients A, B and C can easily be correlated with diffusion coefficients, number and size of cuboids, etc. introduced in Eq. 5.

As pointed out by Schröder et al. [42], $it^{1/2}$ vs. t representations provide a well-defined maximum at a time t_{max} given by:

$$t_{max} = \frac{B^2}{4C^2} = \frac{p^2}{128D_H} \quad (7)$$

Chronoamperometric measurements were performed by applying constant potentials of +550 mV. At this potential, indigo is oxidized to dehydroindigo under diffusion control, and dehydroindigo molecules eventually presented in the specimens do not contribute to the measured current. Plots of $it^{1/2}$ vs. t from chronoamperometric measurements at an applied potential of +550 mV for specimens MBP1, $MBP1_{150}$, MBS1 and $MBS1_{150}$, all after rinsing with

DMSO and acetone, successively are shown in Fig. 4. Remarkably, palygorskite-based specimens provided a response close to that previously reported for Maya Blue samples [16], with a well-defined maximum at t_{max} approximately 4 ms. The response of sepiolite-based specimens was similar, but the maximum in the $it^{1/2}$ function was located at shorter times (approximately 1 ms). As shown in Eq. 3, the value of t_{max} depends on the crystal size and the diffusion coefficient for protons. Although both sepiolite and palygorskite present fibrous patterns when regarded by a electronic microscope, the crystal size (length and diameter of the needle) can be very different, and even the topology of the fibres may be different. This is not only true for the different minerals but also for the same clay, which may present very different crystal sizes, as well as compositional and structural differences depending on its origin, i.e. formation conditions [44]. Even though we have finely grinded both clays with a similar process, the resulting particle sizes may be very different. Both sepiolite and palygorskite can be found in clay form, i.e. where the crystallites are typically less than 2 μm, whose fibres are only seen with the help of an electronic microscope but also in the form of macroscopic fibres visible by eye (mountain leather). Our minerals (Yucatan palygorskite and sepiolite from Yunclillos) correspond to the clay type, but size and topology of microcrystallites may be completely different. Accordingly, the diffusion coefficients for proton and electron transport across the solids may be different, as well as the position of t_{max} in the $it^{1/2}$ vs. t representations.

The analysis of chronoamperometric curves using previously reported parameters for Maya Blue samples [16], lead to D_e and D_H values of 1×10^{-9} and 2×10^{-8} cm^2/s, respectively. Data for sepiolite-based specimens, assuming similar crystal size (which may not be true, as discussed before) lead to $D_e=1\times10^{-9}$ cm^2/s and $D_H=7\times10^{-8}$ cm^2/s. Rigorous analysis of data, however, is even more complicated because: (a) the distribution of indigo molecules within the clay crystals is probably non-uniform or (b) probably there exists a certain degree of anisotropy in the diffusion of electrons and protons through the crystals of these clays.

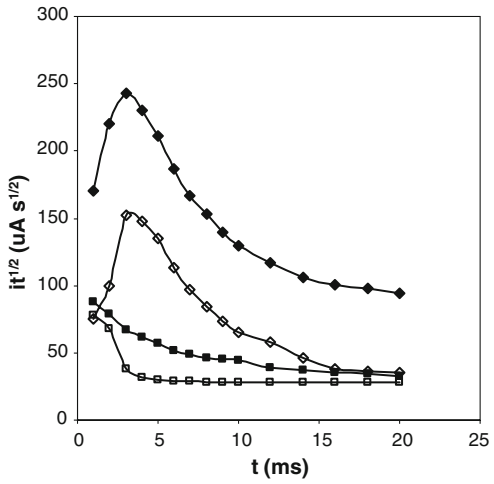

Fig. 4 Plots of $it^{1/2}$ vs. t from chronoamperometric curves recorded at an applied potential of +550 mV at specimen-modified PIGEs in contact with 0.50 M acetate buffer (pH 4.75). *Solid rhombs*, MBP1; *rhombs*, $MBP1_{150}$; *solid squares*, MBS1; *squares*, $MBS1_{150}$, all after rinsing with DMSO and acetone, successively

It should be emphasized that the current can be taken as proportional to the concentration gradient of indigo molecules at the electrode/particle (and the electrolyte/particle) interface, so that, for a uniform distribution of indigo in the crystals, the current becomes proportional to the bulk indigo concentration in the clay, as indicated in Eq. 5.

In order to obtain a rough estimate of the distribution of indigo molecules in palygorskite and sepiolite specimens, an operational approach was used. This is based in the consideration of the variation of the $it^{1/2}$ factor with time, given by:

$$\mathrm{SL}=\frac{\Delta\left(it^{1/2}\right)}{(\Delta t)}=\frac{B}{2t^{1/2}}-C \tag{8}$$

At relatively long times, one can approach SL≈−C, so that, for a uniform distribution of indigo into a uniform set of clay particles, SL must approach a constant value. Since in chronoamperometric experiments, the so-called diffusion layer expands with time, the variation of SL with time should reflect the variation of the 'mean' bulk concentration of indigo with the depth with respect to the electrode/particle interface.

Figure 5 shows plots of SL vs. t for palygorskite- and sepiolite-based specimens derived from chronoamperometric data in Fig. 4. Data at times longer than 2 and 5 ms were used, respectively, for sepiolite- and palygorskite-based specimens in order to consider the time region where SL presumably approaches to −C. Our data correspond to a monotonically decreasing variation of SL with t which, at short times, approaches to linearity. Extrapolation of this nearly linear region gives a value SL_o which can be taken as representative of the indigo concentration at the electrode/particle boundary, $c(0)$. Then, the indigo concentration at a depth x from the surface of the clay crystal, $c(x)$, can be approached by the expression $c(x)/c(0)=\mathrm{SL}/\mathrm{SL_o}$,the corresponding values of x being estimated as the extent of the diffusion layer, given by $x=(\pi Dt)^{1/2}$.

Plots of $c(x)/c(0)$ vs. x are shown in Fig. 6 for different sepiolite- and palygorskite-based specimens after rinsing successively with DMSO and acetone. On comparing the corresponding representations for the different palygorskite- and sepiolite-based specimens, one can obtain that: (a) the concentration of indigo decreases rapid and monotonically

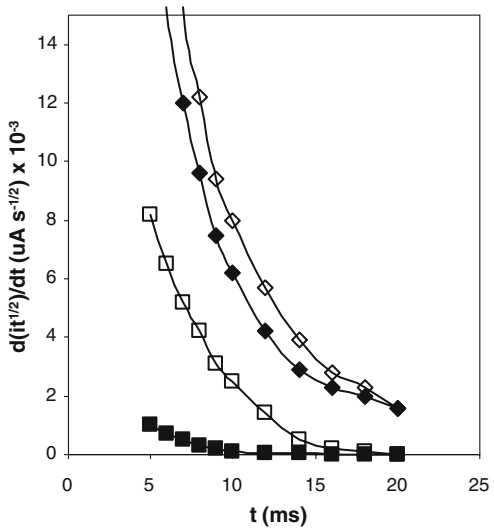

Fig. 5 Plots of SL ($=\Delta(it^{1/2})/\Delta(t)$) vs. t for specimens MBP1 (*solid rhombs*), $MBP1_{150}$ (*rhombs*), MBS1 (*solid squares*) and $MBS1_{150}$ (*squares*) derived from chronoamperograms using conditions described in Fig. 4

with the depth in all cases; (b) the extent of the indigo penetration into the clay is clearly favoured by thermal treatment, but this penetration increases only moderately when the temperature is passed from 130 to 150 and 180 °C; (c) under identical conditions, the penetration increased in the order P1>P2>S2.

Indigo/dehydroindigo relationship

In order to determine the distribution of indigo and dehydroindigo in palygorskite- and sepiolite-based specimens, cyclic voltammetric measurements at different potential scan rates were used. Here, a modification of the method devised by Scholz and Hermes [45] for determining the composition of a system containing a reversibly reducible/oxidable electroactive species in two oxidation states in solution was introduced. This method derives from the fact that the entire CVs for solutions of the reduced and the oxidized forms of the depolarizer, although identical in shape, are shifted along the current axis depending on the redox state. Accordingly, measuring the currents at the lower $i_{\lambda c}$ and upper $i_{\lambda a}$ limits of the potential range, the difference $I = |i_{\lambda a}| - |i_{\lambda c}|$was found to be linearly dependent on the molar ratio of the oxidized (or reduced) form, a_{ox}, of the depolarizer providing that the potential limits are chosen symmetric to the formal potential and that the potential range is at least eight times the peak separation [45]. Extension to solid-state voltammetry is in principle allowed by the fact that, under conditions of large concentration of supporting electrolyte, reversible voltammetric curves for solid-state processes are quite similar to those recorded for species in solution phase [46].

The application of this method is disturbed, apart from deviations from reversibility or eventual coupled reactions in solution, by the presence of ohmic drops in the cell as well as capacitive effects. It is well known [45] that these effects results in distortions of the voltammetric curves, so that compensation with CVs in the absence of depolarizer are eventually needed [45]. Extension to solid-state electrochemistry is in principle allowed in view of the close similarity between the CV responses for species in solution and for ion insertion solids when reversible redox processes occur.

In order to apply this method for determining the dehydroindigo/indigo relationship in Maya Blue specimens, a calibration was performed using CVs for indigo crystals and for indigo attached to montmorillonite and kaolinite (MBMW and MBK specimens). Figure 7 shows a typical

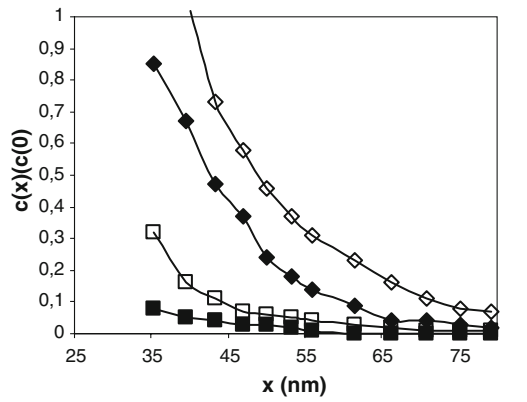

Fig. 6 Plots of $c(x)/c(0)$ vs. x estimated from chronoamperometric data for different palygorskit- and sepiolite-based specimens. Conditions such as in Figs. 4 and 5

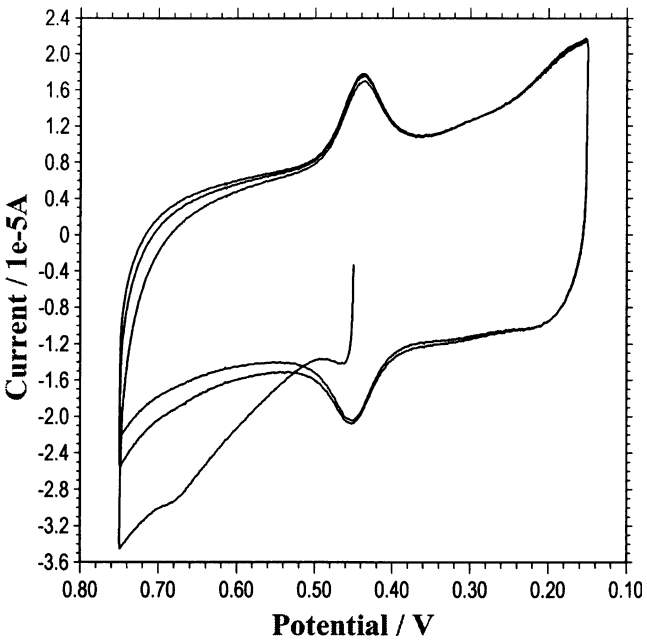

Fig. 7 CV of MBMW attached to PIGE in contact with 0.50 M acetate buffer. Potential scan rate 500 mV/s. The potential is varied 300 mV below and upper the central potential of +450 mV

CV for MBW. In these last systems, indigo is externally adsorbed onto the clay grains, and there is no place for dehydroindigo formation. Then, CVs performed at a central potential of +450 mV correspond to a system with $\alpha_{ox}=0$, while CVs performed at a central potential of −300 mV correspond to systems with $\alpha_{ox}=1$.

Figure 8 shows theoretical calibration plots based on CVs for MBW specimens at potential scan rates ranging from 1 to 10^4 mV/s. Our data indicated that $I = |i_{\lambda a}| - |i_{\lambda c}|$varies significantly with the potential scan rate, an effect associated to voltammogram distortions induced by uncompensated ohmic drops (and eventually capacitive effects), as suggested by large background currents which can be seen in Fig. 7. In order to compensate such effects, the ratio $(|i_{\lambda a}| - |i_{\lambda c}|)/(|i_{\lambda a}| + |i_{\lambda c}|)$, designed in the following as f, was taken. Very similar results were obtained for indigo and MBK specimens. One can see in Fig. 8 that clearly diverging variations of f with the potential scan rate, v, appear. This can be seen in Fig. 9, where the variation of f with the molar fraction of oxidized species at selected v values is depicted. Accordingly, measurements were limited to the 1 to 10^4 mV/s sweep rate range.

As indicated for chronoamperometric experiments, the advance of the diffusion layer through the crystals of the solid is directly related with the characteristic time of the experiment. Roughly, this means that at fast potential scan rates, the CV response will be representative of the composition of the solid in the more external layers of the crystals, while at slow potential scan rates, the composition of more depth regions will be also influential on the electrochemical response.

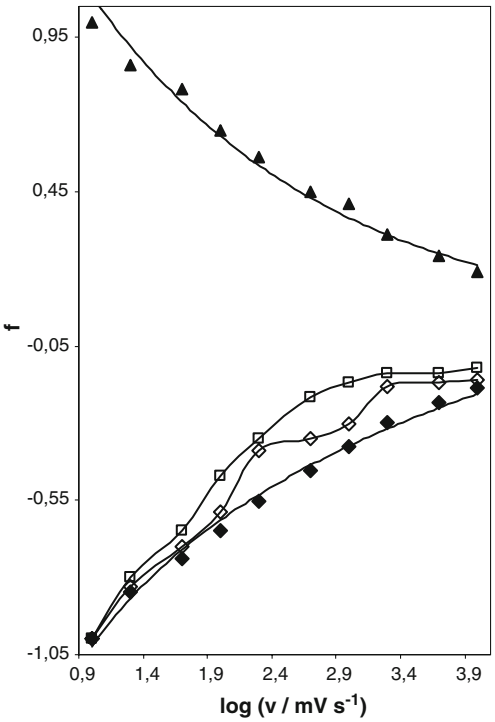

Fig. 8 Calibration plots for the variation of f with the potential scan rate for CVs for MBW specimens immersed into acetate buffer. Central potential: +450 (*solid triangles*) and −300 mV (*solid rhombs*). Switching potentials separated 300 mV from the central potential. Data for $MBP1_{180}$ (*rhombs*) and $MBS1_{180}$ (*squares*) specimens for a central potential=+450 mV

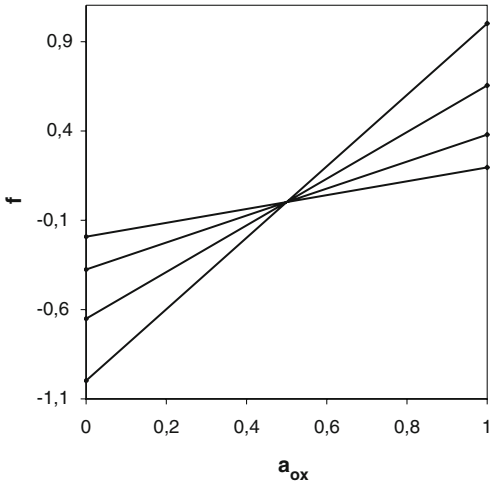

Fig. 9 Calibration plots for the variation of f with the molar fraction of oxidized species in MBMW specimens using CVs in acetate buffer. Conditions such as in Fig. 8. Potential scan rates of 10, 100, 1000 and 10000 mV/s

The variation of f with the potential scan rate v obtained from experimental CV data for $MBP1_t$, $MBP2_t$, $MBS1_t$ and $MBS2_t$ for t=110, 150 and 180 °C after rinsing with DMSO and acetone are illustrated in Fig. 8 for $MBP1_{180}$ and $MBS1_{180}$. In this study, CVs at a central potential of +450 mV (see Fig. 7) were used for quantification. For both sepiolite- and palygorskite-based specimens, at potential scan rates between 10^4 and 10^3 mV/s, the molar fraction of dehydroindigo reaches values close to 20%. For sepiolite-based specimens, this percentage remains almost unchanged at potential scan rates between 10^3 and 2×10^2 mV/s, further decreasing on decreasing the potential scan rate. For palygorskite-based specimens, values of f exhibit two separated maxima at approximately 200 and 2,500 mV/s, as can be seen in Fig. 8. This peculiar feature could be correlated with peak splitting observed in SWVs at low frequencies (vide infra).

This variation of α_{ox} with the potential scan rate can be converted into a α_{ox} vs. x variation taking $x=(D\tau)^{1/2}$. As for chronoamperometric measurements, D represents the diffusion of the rate-limiting charge transport process (here, electron transport across the clay, $D_e=1\times10^{-9}$ cm^2/s) and τ a time characteristic of the experiment. Since in CV, there is no diffusive control along the entire experiment, this characteristic time is not well defined. A reasonable approximation seems to identify t with the time involved in the record of the voltammetric peak, whose potential amplitude is approximately 100 mV. Accordingly, we take τ(s)=100/v (mV/s), v being the potential scan rate of the CV experiment.

The variation of the dehydroindigo/indigo relationship with the depth in the clay crystals estimated for $MBP1_{180}$ and $MBS1_{180}$ specimens is shown in Fig. 10. On comparing CV data for sepiolite-based specimens, one can obtain that: (1) the percentage of dehydroindigo increases from the external surface of the crystals to a depth of 60–80 nm, further decreasing on increasing depth; (2) the maximum percentage of dehydroindigo increases with the temperature of thermal treatment, the larger values being of approximately 28%. Similar results were obtained for palygorskite specimens, where the maximum amount of dehydroindigo was lower, approximately 22%. Remarkably, for palygorskite-based specimens, a secondary maximum of dehydroindigo concentration appeared at a larger depth, approximately 200 nm. As before, it should be noted that depth values are estimated from $D_e=1\times10^{-9}$ cm^2/s. The above feature can be correlated with peak splitting observed in square SWVs at low frequencies (see Fig. 2), thus suggesting that two topological redox isomers are present in this case. On comparing sepiolite- with palygorskite-based specimens, it should be noted that the depth of penetration of indigo is clearly larger in palygorskite than in sepiolite, the depth at which the indigo concentration is close to the 10% of that in the external surface being of 60 and 75 nm, respectively. This is confirmed by cyclic voltammetric data in Fig. 11, corresponding to $MBP1_{180}$ and $MBS1_{180}$ specimens, where the variation of: (a) peak current with the square root of the potential scan rate and (b) the $i_p/v^{1/2}$ ratio with $1/v^{1/2}$ are depicted. Such data reveal significant differences between palygorskite- and sepiolite-based specimens.

These results may be used to explain the much higher resistance of palygorskite–indigo pigments as compared with sepiolite–indigo ones, as reported in [26]. The higher penetration of indigo within the palygorskite crystals as compared with sepiolite ones, together with the much higher resistance of palygorskite to acids [26], could explain the unique properties of Maya Blue (palygorskite plus indigo).

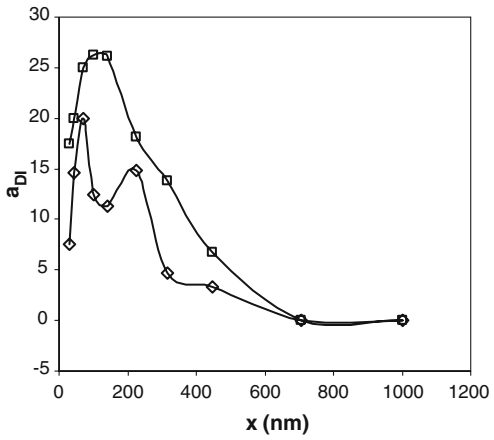

Fig. 10 Variation of the molar fraction of dehydroindigo with the deept in the crystals of $MBP1_{180}$ and $MBS1_{180}$ estimated from data in Fig. 8

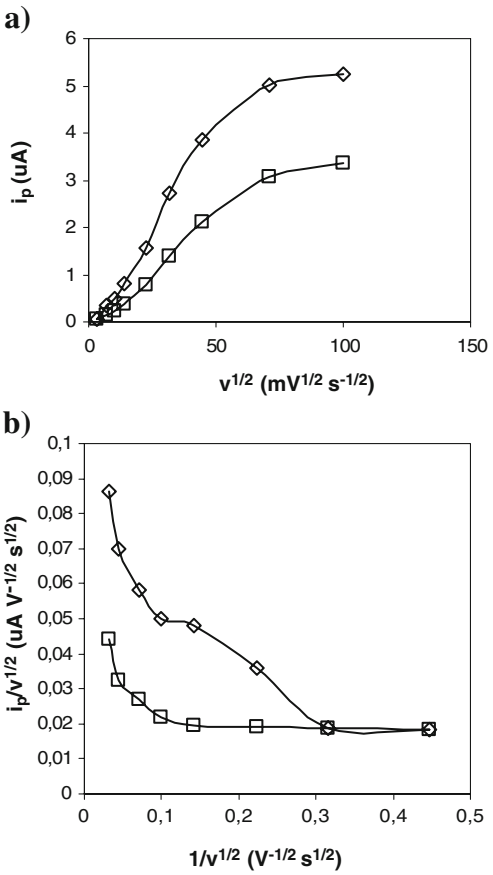

Fig. 11 CV for $MBP1_{180}$ (*rhombs*) and $MBS1_{180}$ (*squares*) samples. **a** Variation of peak current with the square root of the potential scan rate; **b** variation of the $i_p/v^{1/2}$ ratio with $1/v^{1/2}$

Final considerations

The application of the voltammetry of microparticles approach to Maya Blue-type specimens prepared from synthetic indigo and different clays in contact with aqueous electrolytes provides well-defined electrochemical responses. For montmorillonite and kaolinite clays, only external adsorption of indigo occurs, while for palygorskite and sepiolite, the response of externally adsorbed indigo units is superimposed to that of indigo molecules anchored to the aluminosilicate framework. Dehydroindigo accompanies indigo in sepiolite- and palygorskite-based specimens. Both the indigo attachment and the proportion of dehydorindigo increase with the temperature of the thermal treatment during the preparation of specimens.

The combination of chronoamperometric and cyclic voltammetric data allows for estimating the variation of

the concentration of indigo and dehydroindigo with the depth in the clay particles denoting that, in the case of palygorskite, two different topological redox isomers are involved. These data suggest that the existence of a particular anchoring between indigo and phyllosilicate framework, which is not present in the case of sepiolite, could be responsible from the higher resistance of palygorskite–indigo pigments as compared with sepiolite–indigo ones.

These results lead to a further step in the comprehension of Maya Blue as a nanostructured material. It also illustrates how to expanding the capabilities of the voltammetry of micro-particles approach for obtaining information in solid systems.

Acknowledgements Financial support is gratefully acknowledged from the Generalitat Valenciana GV04B/197 and GV04B/441 I+D+I Projects and the MEC projects CTQ2004-06754-C03-01 and 02 and CTQ2006-15672-C05-05, which are also supported with FEDER funds.

References

1. Reyes-Valerio (1993) C De Bonampak al Templo Mayor: el azul Maya en Mesoamérica, Siglo XXI, México
2. Romero P, Sánchez C (2005) N J Chem 29:57–58 doi:10.1039/b416075b
3. Sheppard AO (1962) Am Antiq 27:565–566 doi:10.2307/277680
4. Van Olphen H (1967) Science 154:645–646 doi:10.1126/science.154.3749.645
5. Kleber R, Masschelein-Kleiner L, Tissen J (1967) Stud Conservat 12:41–55 doi:10.2307/1505326
6. José-Yacamán M, Rendón L, Arenas J, Serra Puche MC (1996) Science 273:223–225 doi:10.1126/science.273.5272.223
7. Polette LA, Meitzner G, José-Yacamán M, Chianelli RR (2002) Microchem J 71:167–174 doi:10.1016/S0026-265X(02)00008-5
8. Sánchez del Río MS, Martinetto P, Somogyi A, Reyes-Valerio C, Dooryhée E, Peltier N et al (2004) Spectrochim Acta B 59:1619–1625 doi:10.1016/j.sab.2004.07.027
9. Sánchez del Rio MS, Sodo A, Eeckhout SG, Neisius T, Martinetto P, Dooryhee E et al (2005) Nucl Instrum Methods Phys Res B 238:50–54 doi:10.1016/j.nimb.2005.06.017
10. Chiari G, Giustetto R, Ricchiardi G (2003) Eur J Mineral 15:21–33 doi:10.1127/0935-1221/2003/0015-0021
11. Fois E, Gamba A, Tilocca A (2003) Micropor Mesopor Mat 57:263–272 doi:10.1016/S1387-1811(02)00596-6
12. Hubbard B, Kuang W, Moser A, Facey GA, Detellier C (2003) Clay Miner 51:318–326 doi:10.1346/CCMN.2003.0510308
13. Reinen D, Köhl P, Müller C (2004) Z Anorg Allg Chem 630:97–103 doi:10.1002/zaac.200300251
14. Giustetto R, Llabres i Xamena FX, Ricchiardi G, Bordiga S, Damin A, Gobetto R et al (2005) J Phys Chem B 109:19360–19368 doi:10.1021/jp048587h
15. Giustetto R, Levy D, Chiari G (2006) Eur J Mineral 18:629–640 doi:10.1127/0935-1221/2006/0018-0629
16. Doménech A, Doménech MT, Vázquez ML (2006) J Phys Chem B 110:6027 doi:10.1021/jp0573011
17. Doménech A, Doménech MT, Vázquez ML (2007) Anal Chem 79:2812–2821 doi:10.1021/ac0623686
18. Doménech A, Doménech MT, Vázquez ML (2007) J Phys Chem C 111:4585–4595 doi:10.1021/jp067369g
19. Doménech A, Doménech MT, Vázquez ML (2007) J Solid State Electrochem 11:1335–1346 doi:10.1007/s10008-007-0296-2
20. Scholz F, Meyer B (1998) In: Bard AJ, Rubinstein I (eds) Electroanalytical chemistry, a series of advances. vol. 20. Marcel Dekker, New York, pp 1–87
21. Grygar T, Marken F, Schröder U, Scholz F (2002) Collect Czech Chem Commun 67:63 doi:10.1135/cccc20020163
22. Scholz F, Schröder U, Gulaboski F (2005) Electrochemistry of immobilized particles and droplets. Springer, Berlin
23. Arnold DE, Bohor BF (1975) Archaeology 28:23–29
24. Chisholm JE (1992) Can Mineral 30:61–73
25. Jones BF, Galán E (1988) Sepiolite and palygorskiye. In: Bailey SW (ed) Hydrous phyllosilicates. Reviews in mineralogy. vol. 19. Mineralogical Society of America, Washington, DC, pp 631–674
26. Sánchez del Río M, Martinetto P, Reyes-Valerio C, Doryhée E, Suárez M (2006) Archaeometry 48:115–130 doi:10.1111/j.1475-4754.2006.00246.x
27. Sánchez del Río M, Picquart M, Haro-Poniatowski E, van Elslande E, Uc VH (2006) J Raman Spectr 37:1046–1053 doi:10.1002/jrs.1607
28. Evans JF, Kuwana T (1977) Anal Chem 49:1632–1635 doi:10.1021/ac50019a042
29. Gunasingham H, Fleet B (1982) Analyst (Lond) 107:896–902 doi:10.1039/an9820700896
30. Engstrom RC, Strasser VA (1984) Anal Chem 56:136–141 doi:10.1021/ac00266a005
31. Barisci JN, Wallace GG, Baughman RH (2000) Electrochim Acta 46:509–517 doi:10.1016/S0013-4686(00)00634-4
32. Barisci JN, Wallace GG, Baughman RH (2000) J Electroanal Chem 488:92–98 doi:10.1016/S0022-0728(00)00179-0
33. Bond AM, Marken F, Hill E, Compton RG, Hügel H (1997) J Chem Soc Perkin Trans 2:1735–1742 doi:10.1039/a701003f
34. Grygar T, Kuckova S, Hradil D, Hradilova D (2003) J Solid State Electrochem 7:706–713 doi:10.1007/s10008-003-0380-1
35. Doménech A, Doménech MT (2006) J Solid State Electrochem 10:459–468 doi:10.1007/s10008-005-0018-6
36. Bessel DA, Rolison DR (1997) J Phys Chem B 101:1148–1157 doi:10.1021/jp961716c
37. Doménech A, Formentín P, García H, Sabater MJ (2002) J Phys Chem B 106:574–582 doi:10.1021/jp011315j
38. Doménech A, García H, Alvaro M, Carbonell E (2003) J Phys Chem B 107:3040–3050 doi:10.1021/jp0223657
39. Lovric M, Scholz F (1997) J Solid State Electrochem 1:108–113 doi:10.1007/s100080050030
40. Lovric M, Scholz F (1999) J Solid State Electrochem 3:172–175 doi:10.1007/s100080050144
41. Oldham KB (1998) J Solid State Electrochem 2:367–377 doi:10.1007/s100080050113
42. Schröder U, Oldham KB, Myland JC, Mahon PJ, Scholz F (2000) J Solid State Electrochem 4:314–324 doi:10.1007/s100080000130
43. Doménech A (2004) J Phys Chem B 108:20471–20478 doi:10.1021/jp046831z
44. Suárez M, García-Romero E, Sánchez del Río M, Martinetto P, Doryhee E (2007) Clay Miner 42:287–297 doi:10.1180/claymin.2007.042.3.02
45. Scholz F, Hermes M (1999) Electrochm Commun 1:345 (See corrigendum in Electrochem Commun 2:814 (2000))
46. Lovric M, Hermes M, Scholz F (1998) J Solid State Electrochem 2:402–404